

The stellar (n, γ) cross section of ^{62}Ni

H. Nassar¹, M. Paul^{1*}, I. Ahmad², D. Berkovits³, M. Bettan³, P. Collon⁴, S. Dababneh⁵, S. Ghelberg¹, J.P. Greene², A. Heger⁶, M. Heil⁵, D.J. Henderson², C.L. Jiang², F. Käppeler⁵, H. Koivisto⁷, S. O'Brien⁴, R.C. Pardo², N. Patronis⁸, T. Pennington^{2†}, R. Plag⁵, K.E. Rehm², R. Reifarh⁶, R. Scott², S. Sinha², X. Tang², R. Vondrasek²

¹ *Racah Institute of Physics, Hebrew University, Jerusalem, Israel, 91904*

² *Argonne National Laboratory, Argonne, IL 60439, USA*

³ *Soreq Nuclear Research Center, Yavne, Israel 78800*

⁴ *Physics Department, University of Notre Dame, Notre Dame, IN 46556, USA*

⁵ *Forschungszentrum Karlsruhe Institut für Kernphysik, PF 3640, 76201 Karlsruhe, Germany*

⁶ *Los Alamos National Laboratory, Los Alamos, NM 87545, USA*

⁷ *Department of Physics, University of Jyväskylä, FIN-40351, Finland and*

⁸ *Department of Physics, The University of Ioannina, 45110 Ioannina, Greece*

(Dated: December 2, 2024)

The $^{62}\text{Ni}(n, \gamma)^{63}\text{Ni}$ ($t_{1/2}=100\pm 2$ yrs) reaction plays an important role in nucleosynthesis by controlling the flow path of the slow neutron capture (s -) process. We have determined for the first time the total cross section of this reaction for a quasi-Maxwellian ($kT = 25$ keV) neutron flux. The measurement was performed by a new technique of fast-neutron activation in which accelerator mass spectrometry (AMS) is applied to detect the ^{63}Ni product nuclei. The experimental value of 22.6 ± 2.4 mb differs significantly from predicted values and affects the whole distribution of nuclei with $60 < A < 90$ produced by the weak s -process in massive stars.

PACS numbers: 25.40.Lw, 27.50.+e, 97.10.Tk, 82.80.Ms, 29.40.Cs

The quest for experimentally determined cross sections of stellar nucleosynthesis reactions becomes more focused with the refinement of theoretical models and calculation techniques. Above $A=60$ and except for rare cases, nuclei are created by captures of free neutrons starting from Fe-peak nuclei [1] acting as seeds for the s -process. The path of the weak s -process component, related [2] to helium burning in massive stars of 10 to $25 M_{\odot}$ (M_{\odot} denotes one solar mass), produces mainly isotopes with masses between 60 and 90 and is sketched in Fig. 1 through the neutron-rich Ni region. This component, characterized by a weak neutron exposure but

acting in a massive star, dominates the synthesis of all nuclei beyond the iron peak. The particular importance of the cross section of neutron capture reactions in the Ni region has been emphasized by Rauscher *et al.* [3] who suggest that inaccurate cross section values may be responsible for the overestimate of neutron-rich Ni isotope abundances (compared to solar abundances) in nucleosynthesis calculations. The role of the $^{62}\text{Ni}(n, \gamma)^{63}\text{Ni}$ reaction is critical in this respect because it affects the major part of the weak s -process flow, starting from ^{56}Fe (Fig. 1). In that regime, the neutron exposure is not strong enough to drive the system to the so-called local equilibrium and hence a change in the estimated neutron capture rate of a nucleus, which experiences the entire mass flow, will affect not only the calculated abundance of this nucleus, but also that of all following ones. The experimental information on the $^{62}\text{Ni}(n, \gamma)^{63}\text{Ni}$ reaction cross section at keV energies prior to this work relied on neutron time-of-flight (TOF) measurements aimed at determining resonance parameters [4, 5]. The Maxwellian-averaged capture cross section (MACS) at a thermal energy of $kT = 30$ keV was estimated from these data by [6] (35.5 ± 4 mb) and more recently by [7] as 12.5 ± 4 mb, which is a factor of ~ 3 smaller than in ref.[6]. Moreover, as emphasized in ref.[8], none of these estimates include a possibly significant direct-capture (DC) component. In ref.[8], the $^{62}\text{Ni}(n, \gamma)^{63}\text{Ni}$ MACS up to $kT = 500$ keV is extrapolated from the precisely known thermal-neutron value taking into account a p -wave DC component and the contribution of a sub-threshold resonance; the MACS at $kT = 30$ keV is estimated as 35 ± 5 mb. We report here the first experimental determination of the total $^{62}\text{Ni}(n, \gamma)^{63}\text{Ni}$ cross section for quasi-Maxwellian neu-

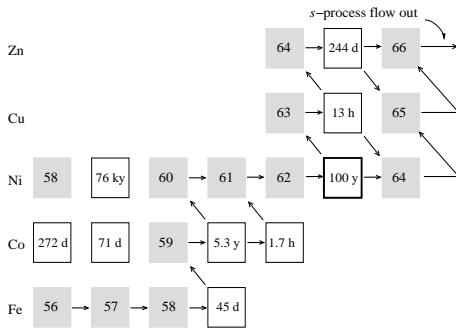


FIG. 1: Main flow of the s -process path starting from ^{56}Fe through the neutron-rich Ni region.

*To whom correspondence should be addressed, email address: paul@vms.huji.ac.il

†Deceased

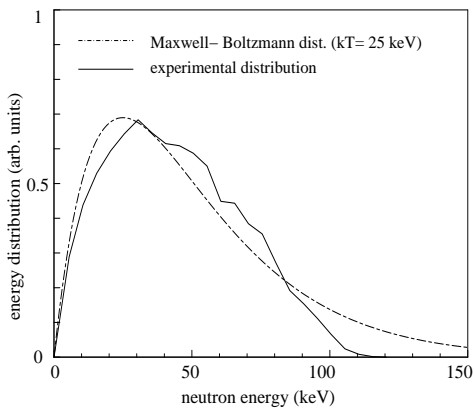


FIG. 2: Neutron energy spectrum measured with the Karlsruhe neutron activation setup. The spectrum is similar to a Maxwellian spectrum at $kT=25$ keV (see text for details).

trons ($kT = 25$ keV). The measurement was performed by a new technique of fast-neutron activation, using accelerator mass spectrometry (AMS). Decay radiation of the long-lived product ^{63}Ni ($t_{1/2} = 100 \pm 2$ yrs) (β^- with an endpoint energy of 66 keV and no γ) is hard or impossible to detect and is replaced in the AMS technique (see [9]) by the detection of ^{63}Ni ions, unambiguously identified after acceleration to several MeV/ u . The MACS $\sigma_V = \langle \sigma v \rangle / v_T$ is extracted from the AMS determination of the isotopic ratio $r = ^{63}\text{Ni}/^{62}\text{Ni} = \sigma_V \langle \phi t \rangle$ in the activated material, using the integrated neutron flux $\langle \phi t \rangle$ monitored during activation.

A 36.8 mg Ni metal sample, enriched to 95% in ^{62}Ni , was activated at the Karlsruhe 3.7 MV Van de Graaff accelerator using a fast-neutron beam obtained from the $^7\text{Li}(p, n)^7\text{Be}$ reaction [10, 11] at a proton energy of 1911 keV, just above threshold. In order to ease the handling of the small sample, the metal powder was dispersed in a camphor matrix and pressed into a pellet; after activation, the metal was recovered (36.2 mg) by subliming the camphor under vacuum. In our conditions, all neutrons are emitted in a forward cone of 120° opening angle and the angle-integrated spectrum provides a good approximation to a thermal spectrum at $kT = 25$ keV, as illustrated in Fig. 2. Before each run, the accelerator was operated in pulsed mode with a repetition rate of 1 MHz and a pulse width of 10 ns. This allowed the measurement of the neutron energy spectra via TOF using a ^6Li glass monitor located 1 m downstream of the ^7Li target. The proton energy is verified via the 106 keV cut-off in the spectrum (Fig. 2). During activation runs, the accelerator was switched to direct-current mode with beam currents around 100 μA . The integrated neutron flux $\langle \phi t \rangle = (3.9 \pm 0.2) \times 10^{15} \text{ cm}^{-2}$, collected over a period of 17.4 days, was continuously monitored by two Au foils sandwiching the sample. In this mode, the ^6Li glass monitor recorded the neutron yield at regular intervals.

The resulting flux history was used to evaluate the corrections for decay of the Au monitors during activation.

To serve as calibration in the AMS measurement, a 321.4 mg high-purity ^{nat}Ni metal powder sample was activated for 30 s at the rabbit facility of the Soreq nuclear reactor in a thermal neutron flux. Au monitors (bare or shielded by a Cd tube), separately activated in the same conditions, yielded a Cd ratio of 10.7 ± 2.3 . After neutron irradiation, the ^{65}Ni (2.5 hrs) γ activity produced in the ^{nat}Ni sample was measured in a 100 cm^3 Ge(Li) detector at a distance of 7.7 cm in order to monitor the integrated neutron flux. The efficiency of the detector was measured, using a vial which contained 0.1413 g of a ^{152}Eu calibrated solution (6.44 ± 0.17 kBq) and reproduced exactly the geometry of the ^{nat}Ni activated sample. The efficiency was determined for the three major γ lines in ^{65}Ni decay (366.3, 1115.5 and 1481.8 keV) by fitting the yields of γ lines in the ^{152}Eu decay at 344.3, 1112.1 and 1408.0 keV, very close in energy to those of ^{65}Ni and including minor corrections for summing effects. From the measured ^{65}Ni activity (corresponding to $(4.58 \pm 0.12) \times 10^9$ (1σ) ^{65}Ni atoms produced in the activation), the thermal-neutron capture and resonance integral of ^{64}Ni ($\sigma_\gamma = 1.52 \pm 0.03$ b and $I_\gamma = 0.98 \pm 0.3$ b [12], respectively) and those of ^{62}Ni ($\sigma_\gamma = 14.2 \pm 0.3$ b, $I_\gamma = 9.6 \pm 3.5$ b [13]), and the isotopic abundances of ^{nat}Ni , we determine a ratio $^{63}\text{Ni}/^{58}\text{Ni} = (7.52 \pm 0.35) \times 10^{-11}$ (1σ) in the reactor-activated ^{nat}Ni sample.

The AMS detection of ^{63}Ni was performed at Argonne National Laboratory, using the Electron Cyclotron Resonance (ECR) ion source [14], acceleration of $^{63}\text{Ni}^{15+}$ ions to 9.2 MeV/ u with the ATLAS facility and the gas-filled magnetic spectrograph technique [15] to separate the extremely intense stable isobaric ^{63}Cu component. A preliminary experiment [16] had shown that feeding of Ni into the ECR plasma chamber in gas phase from nickelocene ($\text{Ni}(\text{C}_5\text{H}_5)_2$) organo-metallic compound reduces the ^{63}Cu contaminant by a factor of ~ 100 compared to solid material. A similar gas-feeding technique was recently used for the detection of ^{63}Ni by AMS using a Cs-sputter negative ion source [17]. For the present experiment, both the fast-neutron and the reactor-neutron activated samples were chemically converted to nickelocene at the University of Jyväskylä [18]. In order to ensure reliable yields in the synthesis process, which required Ni sample masses above ~ 100 mg, the fast-neutron activated sample was mixed with 101.3 mg of high-purity ^{nat}Ni before nickelocene synthesis. The chemical synthesis involving dissolution of the metal in HCl, reaction with NaC_5H_5 , evaporation to dryness and sublimation of $\text{Ni}(\text{C}_5\text{H}_5)_2$, ensured complete isotopic homogenization of the sample; 244.6 mg and 668.5 mg nickelocene from the fast-neutron and reactor-activated samples respectively were obtained. It is important to note that the efficiencies of the chemical procedure or ion production and

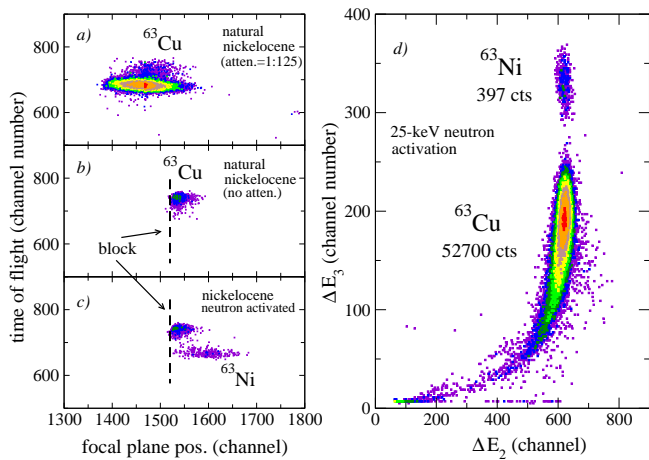


FIG. 3: Gas-filled magnet separation of the ^{63}Cu - ^{63}Ni isobaric pair : *a-c*) Two-dimensional time-of-flight vs. focal plane position spectra for: *a,b*) a ^{nat}Ni (nickelocene) sample in the ECR ion source; *c*) activated ^{nat}Ni . In *a*), the ion beam was attenuated by a factor of 125 to permit the counting of the full ^{63}Cu isobaric group. In *b*) and *c*), most of the ^{63}Cu group is blocked before the detector by a movable shield; *d*) Identification spectrum of ^{63}Ni ions in the detector blocked as in *c*), measured for the fast-neutron activated sample. The x (y) axis represents the energy loss measured in the second (third) anode of the focal-plane ionization chamber.

transport do not affect the measurements of isotopic ratios, assuming that mass fractionation effects therein are negligible. The ATLAS accelerator system was entirely tuned with a stable beam of $^{84}\text{Kr}^{20+}$ prior to the AMS measurement of $^{63}\text{Ni}^{15+}$. The two ions have nearly equal m/q mass-to-charge ratios ($\delta(m/q)/(m/q) = 6.4 \times 10^{-5}$) and are assumed to be transported identically from the ion source to the detection system. The latter was a large hybrid detector composed of a (x, y) position-sensitive parallel-grid avalanche counter (measuring also the ion TOF relative to the accelerator RF trigger) and a multi-anode ionization chamber [19], located in the focal plane of the gas-filled Enge split-pole magnetic spectrograph. The entrance aperture of the detector (48 cm \times 10 cm) ensured 100% acceptance of the ions reaching the focal plane. The spectrograph, filled with N_2 at 20 Torr, focused the ^{63}Ni and ^{63}Cu ions into groups ~ 3 cm wide (FWHM), separated from each other by ~ 5.5 cm (Fig. 3*a-c*). This physical separation allows one to block more than 95% of the extremely intense ^{63}Cu group ($\sim 7 \times 10^4$ ions/s) and let the entire ^{63}Ni group enter into the detector for further discrimination. The latter is achieved by multiple energy-loss measurements along the ion path in the ionization chamber (Fig. 3*d*).

The beam transmission through the accelerator was repeatedly monitored (Fig. 4*a*) during the experiment between sample measurements, by injecting a small amount of isotopically enriched ^{84}Kr gas into the ion source and measuring the ion current at the injection line and be-

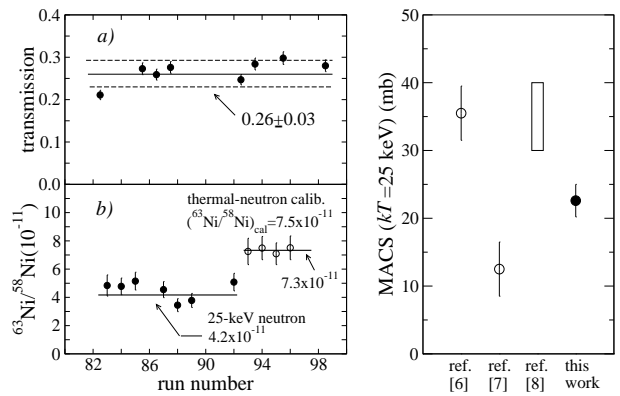


FIG. 4: (left panel): *a*) Beam transmission through the accelerator during the experiment. The abscissa represents the run number. The solid and dashed lines are the unweighted mean and standard deviation of the measured values respectively; *b*) Repeated measurements of the $^{63}\text{Ni}/^{58}\text{Ni}$ ratio for the fast-neutron activated sample (solid dots) and the calibration thermal-neutron activated sample (open dots). The error bar for each run includes (in quadrature) statistical counting error, standard deviation of the mean beam transmission (*a*) and an estimated error on the $^{58}\text{Ni}^{15+}$ mean current during the run (see text). The solid lines indicate the weighted mean of the measurements.

(right panel): Comparison of the present experimental value of the total Maxwellian averaged $^{62}\text{Ni}(n, \gamma)^{63}\text{Ni}$ cross section (solid dot) with theoretical predictions of [6], [7] (open dots) and [8] (open box).

fore the spectrograph. The value and random error adopted for the beam transmission were the unweighted mean and standard deviation of the repeated measurements, respectively. The count rate of identified ^{63}Ni ions (Fig. 3*d*), corrected for beam transmission and for a detection efficiency of 0.90 due to grid shadowing, is divided by the ion current of the stable $^{58}\text{Ni}^{15+}$ beam measured after mass analysis at the accelerator injection line, to yield the $^{63}\text{Ni}^{15+}/^{58}\text{Ni}^{15+}$ isotopic ratio (Fig. 4*b*). An additional correction factor of 0.90 ± 0.04 in the $^{58}\text{Ni}^{15+}$ ion current measured in the injection line was deemed necessary for the fast-neutron activated sample, due to the near degeneracy of $^{58}\text{Ni}^{15+}$ and $^{62}\text{Ni}^{16+}$ beams. This correction was obtained by scanning the intensity of the main Ni isotopes and charge states. It is negligible in the case of the reactor-activated sample which has a very small (natural) ^{62}Ni abundance. In order to reduce unknown systematic errors in the determination of the isotopic ratio described above, the measured isotopic ratios were eventually normalized by the ratio (1.03 ± 0.08) between the values obtained for the reactor-activated sample in the γ and AMS measurements.

From the final determination in the fast-neutron activated (diluted) sample $^{63}\text{Ni}/^{58}\text{Ni} = (4.17 \pm 0.37) \times 10^{-11}$ (weighted mean and standard deviation of the mean of repeated measurements), the number of ^{58}Ni atoms in the sample and the number of ^{62}Ni atoms in the initial

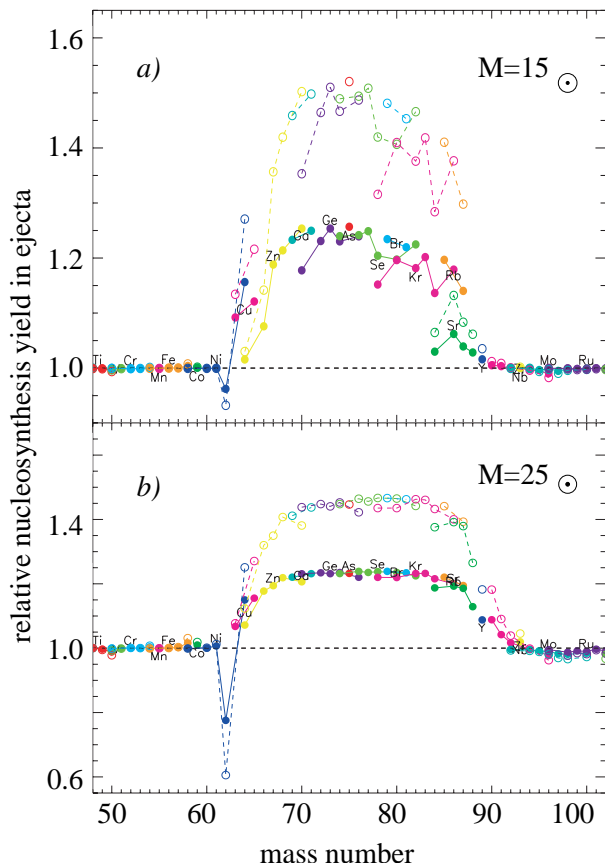


FIG. 5: Nucleosynthesis yields as function of mass number calculated for different values of the $^{62}\text{Ni}(n, \gamma)^{63}\text{Ni}$ cross section and normalized to the yields at a cross section of 12.5 mb [3] for a) a $15 M_{\odot}$ and b) $25 M_{\odot}$ star. Solid dots represent the ratios between the yields calculated using 22.6 mb (this work) to that using 12.5 mb [7]. Open dots represent the ratios between yields for 35 mb [6, 8] and 12.5 mb [7]. Solid (open) dots corresponding to isotopes of a given element are connected by solid (dashed) lines.

^{62}Ni -enriched sample, we derive a ratio $r = ^{63}\text{Ni}/^{62}\text{Ni} = (8.78 \pm 0.79) \times 10^{-11}$. From the relation $r = \sigma_V \langle \phi t \rangle$, we determine a value $\sigma_V(^{62}\text{Ni}) = 22.6 \pm 2.4$ mb for the $kT = 25$ keV Maxwellian-averaged total neutron capture cross section of ^{62}Ni . This value differs significantly from existing theoretical predictions (Fig. 4, right panel).

Figure 5 compares the results of stellar-evolution calculations using different values of $\sigma_V(^{62}\text{Ni})$ relative to the results of models S15 and S25 of ref.[3] for a $15 M_{\odot}$ and $25 M_{\odot}$ star respectively. All calculations assumed the same temperature dependence [3, 7] of the reaction rates and differed solely by the value adopted for $\sigma_V(^{62}\text{Ni})$ at $kT = 25$ keV : 22.6 mb (this work), 12.5 [3, 7] or 35.5 mb [6]. The mass region $60 < A < 90$ exhibits the characteristic abundance peak due to s -process nucleosynthesis in massive stars [2]. These s yields are strongly influenced by the change in $\sigma_V(^{62}\text{Ni})$. The dip in Fig. 5 indicates that the net production of ^{62}Ni itself is damped by the larger cross section value. Together with this, its effect of

bottle neck in the reaction flow between the major seed nuclei ^{56}Fe , ^{58}Ni and the mass region beyond $A = 63$ is reduced. As the ^{62}Ni cross section increases from 12 mb [7] to the present value of 22.6 mb, the overall s -process yield is enhanced by $\sim 20\%$. This trend, which amplifies the overproduction in this region compared to solar abundances already noted in ref.[3], underlines that – in addition to the need for a better assessment of the rate of the neutron-producing reaction $^{22}\text{Ne}(\alpha, n)^{25}\text{Mg}$ [20] – the cross section data for the potential bottle neck nuclides ^{58}Fe and ^{60}Ni must be verified as well. Such an update of the required data set appears to be mandatory for describing the s -process abundances from massive stars, which represent an important contribution to the chemical history of the universe.

This work was supported in part by the US-DOE, Office of Nuclear Physics, under Contract No. W-31-109-ENG-38 and by the USA-Israel Binational Science Foundation (BSF). A.H. and R.R. performed this work under the auspices of the U.S. Department of Energy at the Los Alamos National Laboratory operated by the University of California under contract No. W-7405-ENG-36.

-
- [1] C. Sneden and J.J. Cowan, *Science* **299**, 70 (2003).
 - [2] C.M. Raiteri *et al.*, *Astrophys. J.* **419**, 207 (1993).
 - [3] T. Rauscher *et al.*, *Astrophys. J.* **576**, 323 (2002).
 - [4] H. Beer, R.R. Spencer and A. Ernst, *Astron. Astrophys.* **37**, 197 (1974).
 - [5] H. Beer and R.R. Spencer, *Nucl. Phys.* **A240**, 29 (1975).
 - [6] Z.Y. Bao and F. Käppeler, *At. Data Nucl. Data Tables* **36**, 411 (1987).
 - [7] Z.Y. Bao *et al.*, *At. Data Nucl. Data Tables* **76**, 70 (2000).
 - [8] T. Rauscher and K. H. Guber, *Phys. Rev. C* **66**, 028802 (2002).
 - [9] C. Tuniz, J.R. Bird, D. Fink and G. F. Herzog. *Accelerator Mass Spectrometry - Ultrasensitive Analysis for Global Science*. CRC Press, ISBN 0-8493-4538-3, Boca Raton, Florida (1998).
 - [10] H. Beer and F. Käppeler, *Phys. Rev. C* **21**, 534 (1980).
 - [11] W. Ratynski and F. Käppeler, *Phys. Rev. C* **37**, 595 (1988).
 - [12] E. Gryntakis, *J. of Radioanal. Chem.* **46**, 159 (1978).
 - [13] G.H.E. Sims and D.G. Juhnke, *J. Inorg. Nucl. Chem.* **32**, 2839 (1970).
 - [14] M. Schlapp *et al.*, *Rev. Sci. Instr.* **69**, 631 (1998).
 - [15] M. Paul *et al.*, *Nucl. Instr. and Meth. A* **277**, 418 (1989).
 - [16] H. Nassar *et al.*, *Proc. 6th Int. Conf. on Radioactive Nuclear Beams*, 22-26 Sep, 2003, Argonne, Ill., USA (2003).
 - [17] T. Straume *et al.*, *Nature* **424**, 539 (2003).
 - [18] H. Koivisto, J. Ärje and M. Nurmi, *Nucl. Instr. and Meth. B* **94**, 291 (1994).
 - [19] M. Paul, B. Harss, D. Henderson, C.L. Jiang and K.E. Rehm, *Physics Division Ann. Rep.*, ANL-97/14, p. 79 (1997).
 - [20] M. Jaeger *et al.*, *Phys. Rev. Lett.* **87**, 202501 (2001).